

Fabricating Copper Components with Electron Beam Melting

▶ **P. Frigola**
RadiaBeam
Technologies LLC
Santa Monica, Calif.

▶ **O.A. Harrysson**
T.J. Horn
H.A. West*
R.L. Aman
J.M. Rigsbee,
FASM*
Center for Additive
Manufacturing and
Logistics
North Carolina State
University, Raleigh

▶ **D.A. Ramirez**
L.E. Murr, FASM*
F. Medina
R.B. Wicker
E. Rodriguez
W.M. Keck Center
for 3D Innovation
University of Texas,
El Paso

The ability to make components from copper and copper alloys via additive manufacturing is spurring a range of novel applications.

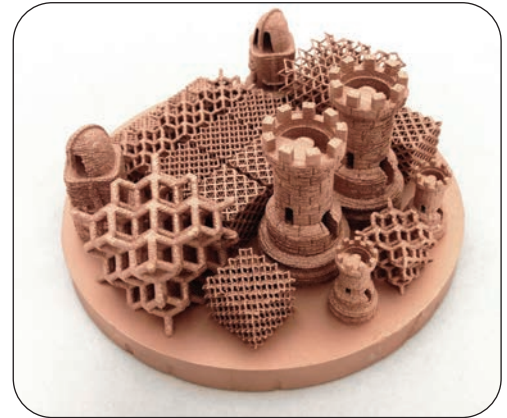
Direct fabrication of fully dense metal structures using the electron beam melting (EBM) process developed by Arcam AB, Sweden, has been successfully demonstrated for a wide range of materials including Ti-6Al-4V^[1,11,9], cobalt chromium^[7,6], titanium-aluminide^[4,8], H-13 steel^[2], and nickel-base alloys^[10]. A growing interest in additive manufacturing (AM) to build components from copper and copper alloys^[5,13,12] is spurring a variety of applications including novel radio frequency (RF) accelerating structures.

A critical issue for high average power, high brightness photoinjectors—the technology of choice for generating high brightness electron beams used in many of today’s linear accelerators—is efficient cooling. RadiaBeam Technologies is exploring the use of AM to fabricate complex RF photoinjectors with geometries optimized for thermal management: Spatially optimized internal cooling channels can be fabricated without the constraints typically associated with traditional manufacturing methods.

However, several properties of pure copper present significant processing challenges for direct metal AM. For one, pure copper has a relatively high thermal conductivity (401 W•m⁻¹•K⁻¹ at 300K) which, while ideal for thermal management applications, rapidly conducts heat away from the melt area resulting in local thermal gradients. This can lead to layer curling, delamination, and ultimately, build and part failure. Additionally, copper’s high ductility hinders post-build powder removal and recovery. Particles also tend to agglomerate, reducing overall flowability and impeding powder deposition. Because Cu is sensitive to oxidation, great care must be taken in handling and storage before, during, and after part fabrication.

Fabrication methods

Initial experiments focused on developing stable parameters for processing copper using EBM. An Arcam model S12 at North Carolina State University, and an Arcam model A2 at the University of Texas El Paso, fabricated the samples for these experiments. EBM hardware is described elsewhere in detail^[3,4,5,6]. A circular start plate made of oxygen free, high conductivity (OFHC) copper measuring approximately 150 x 10 mm leveled on a 10-mm-thick bed of loose



copper powder was the build substrate. Initially, the electron beam scans the start plate surface at high power and high speed, raising the plate temperature to 500°-600°C. Fast scan rates allow maintenance of a relatively high temperature throughout the build process, reducing internal stresses caused by thermal gradients.

Processing each layer typically requires two separate parameter steps called *themes*, which contain all of the required process parameters, such as beam speed and power, and focus offset. The first step is *preheating*, which raises the powder temperature and causes it to lightly sinter together. This mechanical bond facilitates the next step, *melting*, which is divided into two sub-steps: *contours* and *hatching*. The contours step uses relatively low current and speed to trace the outline of each layer with a proprietary control step called *multi-beam*, which uses the high scan rate capabilities to jump between multiple locations on the contour, approximating multiple beams that are able to simultaneously maintain multiple (~60) melt pools. This approach improves surface finish compared to single-spot contouring while maintaining productivity. In the hatching step, beam current and speed are increased and the beam is rastered to melt the area between contours. With each layer, the hatch direction is rotated 90° and spacing between hatch lines is offset by 0.05 mm.

EBM process parameters

Preliminary efforts in parameter development focused on evaluating and optimizing powder raw material. Powders from three manufacturers were obtained. Two high-purity 99.99% Cu powders (A and B) were atomized in argon, while a third low-purity 99.8% Cu

*Member of ASM International

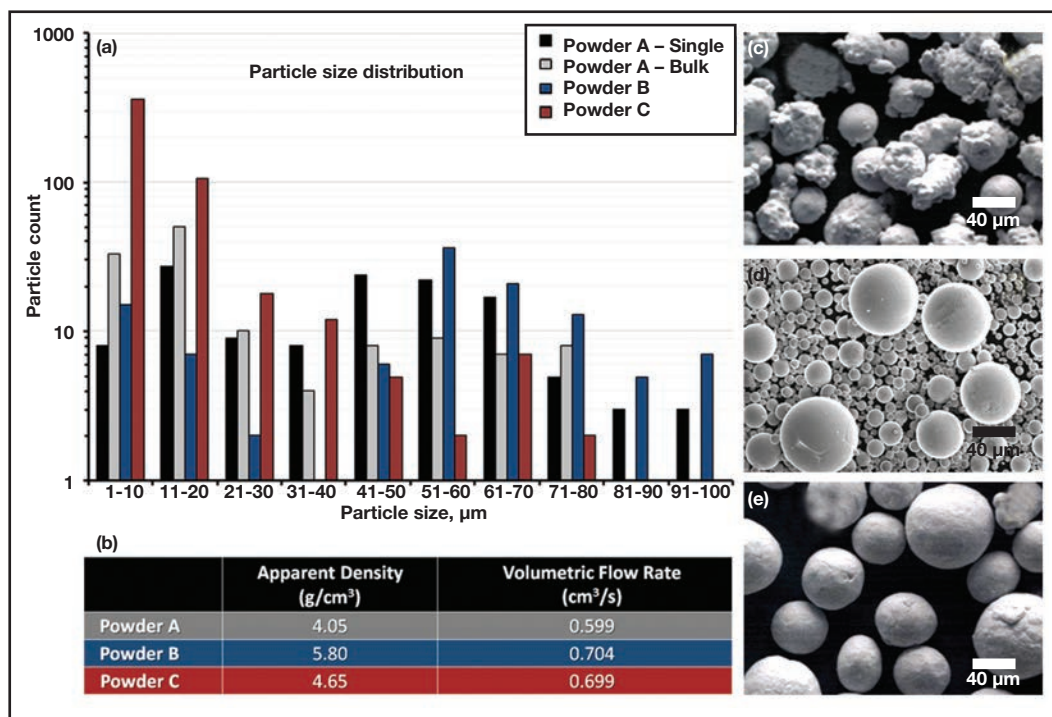


Fig. 1 — Measurements of particle size distribution for each powder type (1a). Table defines average apparent density and average volumetric flow time (1b). Micrographs show shapes of three different powder types—powder A (1c), powder B (1d), and powder C (1e).

powder (C) was atomized in air. Particle morphology and size distribution are important considerations in developing EBM process parameters. Figure 1a shows two distributions for powder A—one separating the satellite particles from the distribution measurement, and one including them in the overall particle diameter. Powder B has a skewed distribution with small particles, while powder C shows a bimodal distribution with an average size of roughly 55 μm . Particles that are too large are not deposited by the raking system, while those that are too small may be charged and scattered by the beam and may also require special handling and storage considerations. The relative packing density, as well as the contact area between particles, can have a significant influence on flowability, thermal conductivity, and melt pool liquid flow. Apparent density and volumetric flow rate of the three high-purity copper powder types, shown in Fig. 1b, were analyzed according to ASTM standards B703-10 and B855-06, respectively^[14,15]. An Arnold meter consistently measured equal volumes of powder. Flow time (in seconds) of the sample was then measured using a calibrated Hall flowmeter.

Subsequent microscopic analysis explains some of the differences in flow times and apparent densities for the different powders. Powder A particles, shown in Fig. 1c, are irregularly shaped and exhibit a higher flow time than powder B and C particles, which are nearly spherical. For particles of relatively equal size, improved flow tends to come at the cost of reduced packing. For all powder types, another cause of poor flow characteristics involves small satellite particles attached to the surface of larger ones.

Microstructural and elemental powder analysis

All powder samples were mounted, ground, polished (0.03 μm alumina), and etched using a solution of 100 mL water, 8 mL sulfuric acid, 4 mL sodium chloride, and 2 g potassium perchlorate. For imaging, a Reichart MF4 A/M optical metallograph with digital image converter was

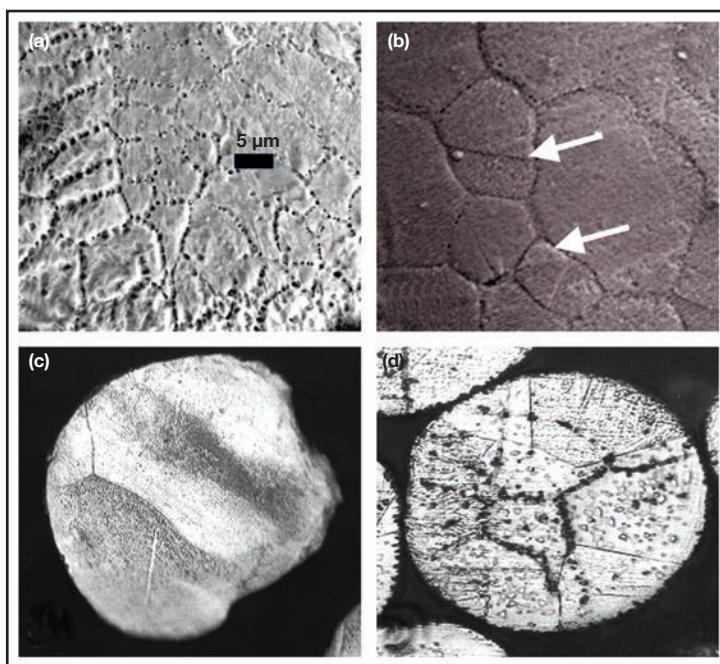


Fig. 2 — Magnified SEM image of powder C section showing high concentration of oxides at the grain boundaries (a), and powder B section showing some oxides at the grain boundaries indicated by arrows (b). Optical microscopy views of embedded, polished, and etched Cu particles of powder B, new (c) and used after several EBM build cycles (d), showing a nearly equiaxed grain structure with increased oxygen in the grain boundaries.

used. Polished and etched samples were also observed in a Hitachi H-8500 field emission SEM. Residual Vickers microindentation hardness values were measured in a Struers DORAMIN A-300 digital test station.

Oxygen content in the powder plays a significant role in the EBM process. The three powders were analyzed for oxides and it was found that powders A and C had the greatest concentration due to the manufacturing processes used. Figure 2a shows an SEM image of a cross-section for a powder C particle with small equiaxed grains with no-

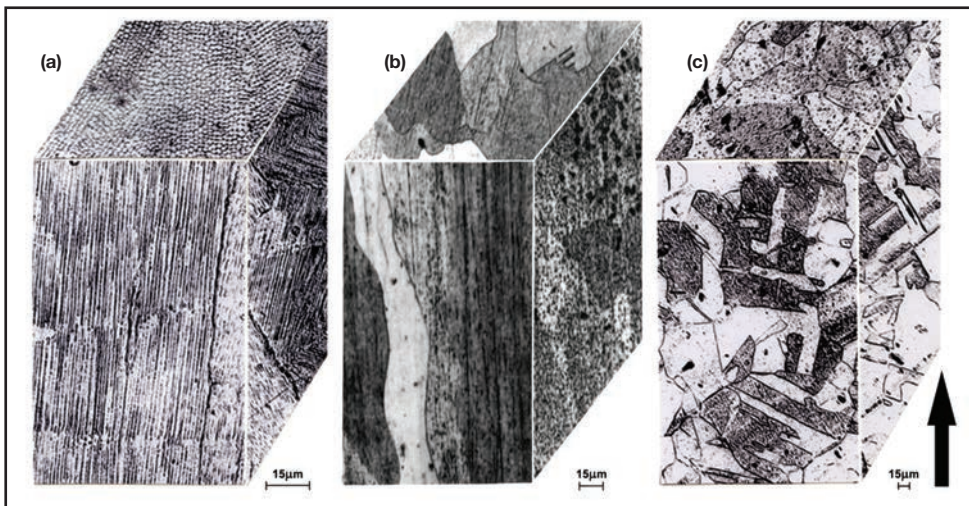


Fig. 3 — 3D construction shows EBM-built Cu components from a mixture of 99.80% Cu powder C and a prior, high oxide powder A (a); 99.99% Cu powder B (b); and 99.99% Cu powder B built at elevated temperature (c). Arrow denotes build direction.

point for subsequent parameter optimization. The EBM process was operated in automatic mode, in which parameters such as beam current and speed are calculated for each layer and adjust with changes in part geometry to maintain a stable process. The desired surface temperature is specified and a “speed function” is selected.

Both substrate starting temperature and desired surface temperature are critical for the build, as over-melting or over-sintering makes powder recovery difficult or impossible. These temperatures also affect surface quality, porosity, and microstructure. The speed function is a parameter that adjusts beam rate during hatching, with higher values resulting in higher beam speeds. Other adjusted parameters include hatch spacing and contours functions. An experiment was designed where 24 cylinders in six builds were fabricated with 24 different sets of process parameters. The goal was to find a set of process parameters to produce fully dense copper cylinders with an acceptable surface finish and desired microstructure.

Early experiments resulted in cylinders with severe delamination, hypothesized to be caused by a significant thermal gradient within each layer. The high thermal conductivity of the copper powder (particularly after sintering/melting) was suspected to be the cause. To balance heat transfer throughout the build area, three stainless steel plates (210 × 210 × 10 mm) were installed under the copper start plate. After analyzing all specimens, a parameter set was developed to consistently produce acceptable parts. From this theme, samples were prepared for examination of metallurgical, mechanical, thermal, and electrical properties. Finally, prototypes of the RF photoinjector were fabricated for field testing.

Sample evaluation

Figure 3 shows corresponding and comparative 3D optical metallographic image composites illustrating oxide influenced, directionally solidified microstructures or microstructural architectures. In Fig. 3a, using a mixture of the high-oxide containing powder C and powder A, EBM processing produces columnar oxide architectures oriented in the build direction (arrow). In contrast, Fig. 3b shows columnar grain structures intermixed with columnar oxides when the high-purity powder B was employed. In Fig. 3c, powder B was again used to build a smaller com-

TABLE 1 — SUMMARY OF MEASURED EBM FABRICATED COPPER MATERIAL PROPERTIES

	EBM Ti6Al4V [*]	Wrought Ti6Al4V (ASTM F1472)	EBM Copper	Wrought C10100 Copper
Density	>99.9%	—	8.84 g/cm ³	8.90 g/cm ³
Electrical conductivity @ 20°C	—	—	97% IACS	102% IACS
Thermal conductivity	—	—	390 W/m*K	391 W/m*K
Yield strength (Rp 0.2)	950 MPa	860 MPa	76 MPa	69 MPa

Summary of measured EBM-fabricated copper material properties compared to wrought copper and the Arcam-developed titanium alloy.

^{*}Arcam Ti6Al4V Material Data Sheet, (www.arcam.com/CommonResources/Files/www.arcam.com/Documents/EBM%20Materials/Arcam-Ti6Al4V-Titanium-Alloy.pdf)

table oxide (Cu₂O) in the grain boundaries and a corresponding SEM image for 99.99% Cu powder B (Fig. 2b) with a lower density of grain boundary oxides (arrows). While the atomization and rapid solidification of the powder manufacturing process itself incorporates various oxide concentrations, residual oxygen and water vapor in the EBM system is also absorbed in the unconsolidated powder during processing. This feature is shown in Figs. 2c and 2d, which compare optical metallographic cross-section views for the initial (precursor) powder B and used powder particles, showing recognizably increased oxides at the grain boundaries.

Evident from these figures is that the powder parameters (especially the oxide or oxygen content), combined with the EBM build parameters, must be carefully considered in order to fabricate products with desirable properties, particularly high electrical conductivity.

EBM processing of copper samples

Powder A was selected for further study. Although this powder exhibited relatively poor raking characteristics due to its irregular shape, its significantly lower cost made it an attractive candidate for EBM parameter development. EBM parameters were assigned to each cylinder based on a previous feasibility study^[5] designed to provide a starting

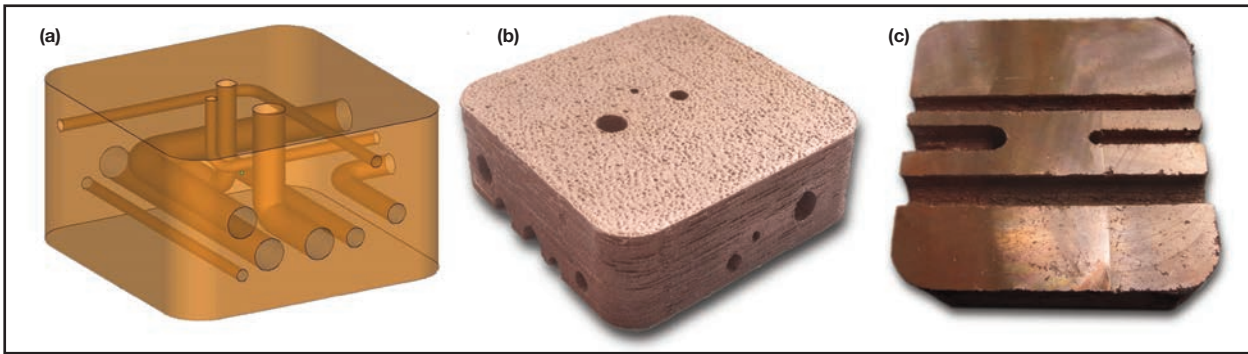


Fig. 4 — 3D CAD model of the cooling channel test block shows internal cooling channel geometry (a); photographs of the sectioned EBM-fabricated test blocks show cooling channels of 1.5, 4, and 7 mm in diameter (b and c).

ponent than in Fig. 3b and the part temperature was considerably higher, producing a component with a more conventional Cu equiaxed grain structure containing coherent annealing twins. This structure does not show any directionally solidified microstructure.

Table 1 shows initial testing results of the physical properties. Bulk thermal conductivity (W/m^*k) measurements were recorded at ambient conditions using the ThermTest TPS 2500S thermal constants analyzer (ISO/DIS 22007-2.2). Electrical conductivity (% IACS), also carried out in ambient conditions, was measured with a Verimet Eddy current conductivity meter. Tensile testing was carried out on ASTM E8 subsize specimens fabricated in the XYZ and XZY orientations per ASTM F2921.

Prototype fabrication and field testing

The final step in this feasibility study was to demonstrate the ability to fabricate a complex geometry that incorporates internal cooling channels. The block shown in Fig. 4 was fabricated with three different channel sizes running straight through the part in three orthogonal directions that curve through the part with 90° elbows. This design also demonstrates the ability to clean sintered powder from internal cooling channels.

Cathode high power RF testing

In order to verify RF performance of the EBM copper, a copper cathode suitable for testing in the UCLA Pegasus 1.6 cell photoinjector also was fabricated using the process parameter sets developed during initial experiments. An example is shown in Fig. 5. Figure 5 also shows the cathode in the as-EBM condition, after final machining, and being installed in the Pegasus photoinjector (Fig. 5e). No other heat treatment was carried out on the EBM cathode prior to final machining.

The EBM copper cathode performed as well as other

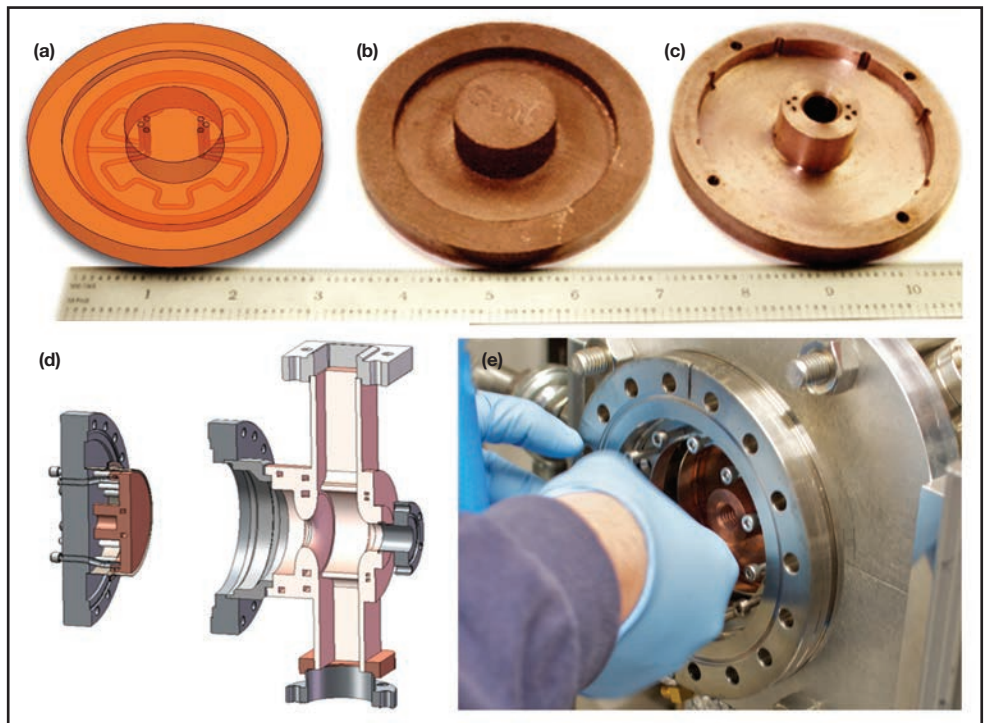



Fig. 5 — CAD rendering shows internal cooling channels of proposed EBM fabricated cathode offered as a standard drop-in replacement by RadiaBeam (a); photograph of the cathode blank in the as-EBM condition (b), and after final machining (c); CAD rendering of the RadiaBeam prototype freeform cathode and freeform photoinjector (d); and installation in the UCLA Pegasus 1.6 cell Photoinjector (e).

cathodes conventionally machined from wrought oxygen-free (OFE) copper material during high power RF testing. Stable operation with 70 MV/m peak electric fields on the cathode was achieved after two hours of RF conditioning. A photoelectron beam with energy of 3.3 MeV and charge of 60 pC was measured, along with a cathode quantum efficiency of $\sim 2 \times 10^{-5}$. These numbers are consistent (given the operating gradient) with conventional OFE copper cathodes measured in the past at the Pegasus Laboratory.

Conclusions

Although the high thermal conductivity of copper presents challenges for direct AM processes, fully dense copper components with complex geometries were demonstrated. Of particular interest is the ability to fabricate internal cooling channels and mesh structures to optimize thermal management. In addition to EBM processing parameters, oxidation of the copper powder was found to hinder the ability to make completely suc-

cessful parts. Higher vacuum and care in the reuse of powder is a critical concern because high oxygen or dense oxide content produces columnar oxide architectures, which may significantly affect both thermal and electrical conductivity. 

For more information: Timothy J. Horn is a research scholar, Center for Additive Manufacturing and Logistics, North Carolina State University, 111 Lampe Dr., 126 Daniels Hall, Raleigh, NC 27607, 919.961.6296, tjhorn.ims@gmail.com, camal.ncsu.edu.

Acknowledgments

This work was supported by DOE SBIR Grants DE-SC0000867 and DE-SC0000869. The authors would also like to thank Pietro Musumeci, Renkai Li, Hos To, and James Rosenzweig for hosting and conducting the RF tests of the photo-cathode at the Particle Beam Physics Laboratory at UCLA.

References

1. D. Cormier, et al., Characterization of Thin Walled Ti-6Al-4V Components Produced via Electron Beam Melting, Proceedings of the Solid Freeform Fabrication Symposium, p 440-447, 2004.
2. D. Cormier, et al., Characterization of H13 Steel Produced via Electron Beam Melting, *Rapid Prototyping J*, Vol 10.1, p 35-41, 2004.
3. D. Cormier, O. Harrysson, and H. West. Characterization of High Alloy Steel Produced via Electron Beam Melting, Proceedings of the Solid Freeform Fabrication Symposium, p 548-558, 2003.
4. D. Cormier, et al., Freeform Fabrication of Titanium Aluminide via Electron Beam Melting Using Prealloyed and Blended Powders, *Research Letters in Mat. Sci.*, p 1-4, 2007.
5. P. Frigola, et al., A Novel Fabrication Technique for the Production of RF Photoinjectors, Proceedings of EPAC08, Genoa, Italy, p 751-753, 2008.

6. S.M. Gaytan, et al., Comparison of Microstructures and Mechanical Properties for Solid and Mesh Cobalt-Base Alloy Prototypes Fabricated by Electron Beam Melting, *Metall. Mater. Trans. A*, Vol 41A, p 3216-3227, 2010.
7. O. Harrysson, et al., Direct Fabrication of Metal Orthopedic Implants Using Electron Beam Melting, Proceedings of the Solid Freeform Fabrication Symposium, p 339-446, 2003.
8. L.E. Murr, et al., Characterization of Titanium Aluminide Alloy Components Fabricated by Additive Manufacturing Using Electron Beam Melting, *Acta Mater.*, Vol 58, p 1887-1894, 2010.
9. L.E. Murr, et al., Next Generation Biomedical Implant Using Additive Layer Manufacturing of Complex, Cellular and Functional Mesh Arrays, *Philos. T. Roy. Soc. A*, Vol 368, p 1999-2032, 2010.
10. L.E. Murr, et al., Microstructural Architecture, Microstructures and Mechanical Properties for a Nickel-Base Superalloy Fabricated by Electron Beam Melting, *Metall. Mater. Trans. A*, Vol 42, p 3491-3508, 2011.
11. L.E. Murr, et al., Microstructure and Mechanical Behavior of Ti-6Al-4V for Biomedical Applications Produced by Rapid Layer Manufacturing, *J. Mech. Behavior Biomed. Mater.*, Vol 2, p 20-32, 2009.
12. D.A. Ramirez, et al., Open-Cellular Copper Structures Fabricated by Additive Manufacturing Using Electron Beam Melting, *Mater. Sci. and Eng. A*, J28A: 5379-5386, 2011.
13. D.A. Ramirez, et al., Novel Precipitate-Microstructural Architecture Developed in the Fabrication of Solid Copper Components by Additive Manufacturing Using Electron Beam Melting, *Acta Mater.*, Vol 59, p 4088-4099, 2011.
14. Standard Test Method for Apparent Density of Free-Flowing Metal Powders and Related Compounds using the Arnold Meter: ASTM B 703-10.
15. Standard Test Method for Volumetric Flow Rate of Metal Powders Using Arnold Meter and Hall Funnel: ASTM B 855-06.



Register Today!

AEROSPACE COATINGS CONFERENCE AND EXPOSITION

Development and Manufacturing Trends for the 21st Century

October 8-9, 2014 • Hartford, Connecticut, USA

This interactive experience in the heart of "aerospace alley" brings together thermal spray professionals, from sprayers to coating designers, to discuss current and future trends in the manufacturing of aerospace coatings.

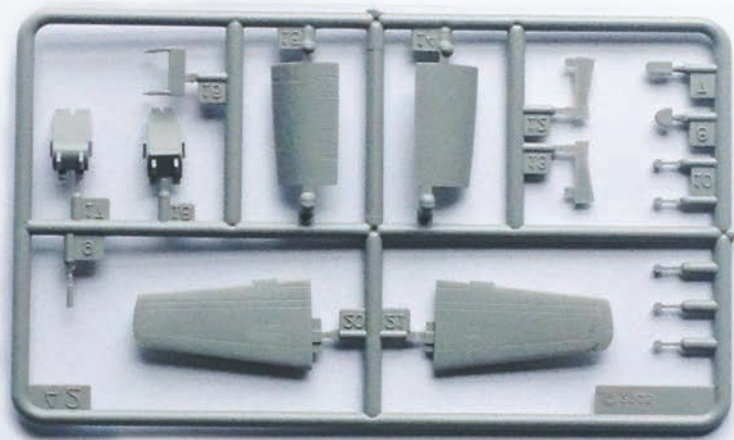
Register now for this highly collaborative event where you can exchange information to best understand future OEM requirements and trends.

Check our website often for Early Bird registration pricing and other important information.

www.asminternational.org/aerospacecoatings

Interested in exhibiting and sponsorship opportunities?

Contact Kelly Thomas, Global Manager, Sales & Expositions at 440.338.1733 or kelly.thomas@asminternational.org



Organized By:

